

Magnetic phase separation in EuB_6 detected by muon spin rotation

M. L. Brooks,¹ T. Lancaster,¹ S. J. Blundell,¹ W. Hayes,¹ F. L. Pratt,² and Z. Fisk³

¹*Clarendon Laboratory, University of Oxford, Parks Road, Oxford OX1 3PU, United Kingdom*

²*ISIS Muon Facility, ISIS, Chilton, Oxon. OX11 0QX, United Kingdom*

³*Department of Physics, University of California, Davis, Davis, CA 95616*

(Dated: November 27, 2018)

We report results of the first muon-spin rotation measurements performed on the low carrier density ferromagnet EuB_6 . The ferromagnetic state is reached via two magnetic transitions at $T_m = 15.5$ K and $T_c = 12.6$ K. Two distinct components are resolved in the muon data, one oscillatory and one non-oscillatory, which arise from different types of magnetic environment, and we have followed the temperature dependence of these components in detail. These results provide evidence for magnetic phase separation and can be interpreted in terms of the gradual coalescing of magnetic polarons.

PACS numbers: 76.75.+i, 75.47.Gk, 75.50.Cc

Europium hexaboride has attracted recent interest because it exhibits colossal magnetoresistance (CMR)¹ and it has been suggested that its semiconductor-semimetal transition results from the overlap of magnetic polarons². EuB_6 crystallises into a simple cubic structure (space-group $Pm\bar{3}m$) with divalent Eu ions ($^8S_{7/2}$) at the corners of the unit cell and B_6 -octahedra at the body-centred positions, and is a ferromagnet at low temperatures¹. Specific heat and magnetization measurements reveal that this state is reached via two distinct transitions at $T_m = 15.5$ K and $T_c = 12.6$ K^{2,3}. Neutron diffraction measurements show that a small spontaneous magnetic moment begins to grow on cooling below T_m , but does not become significant until T_c is reached, below which point the moment shows a more usual mean-field like behaviour⁴. The magnetic ordering is accompanied by a sharp drop in the resistivity which is strongly field dependent⁵ and gives rise to a large negative magnetoresistance². This transition from a semiconductor at high temperatures to a semimetal^{6,7,8,9} (or possibly a self-doped compensated semiconductor¹⁰) at low temperatures is reminiscent of the metal-insulator transition seen in manganites exhibiting CMR¹¹. Detailed measurements of resistivity and magnetization² show that this transition is associated with T_m . It is thought that magnetic polarons could be responsible for this behaviour, with the upper magnetic transition and drop in resistivity caused when the bound carriers overlap and percolate, and the lower transition caused by a true transition to a bulk ferromagnetic state². Further support for this explanation comes from the observation of polaronic features, possibly associated with itinerant holes¹², below ~ 30 K in Raman-scattering spectra¹³. The trapping of carriers to form bound magnetic polarons provides an explanation for the upturn in resistivity observed on cooling through 30 K^{2,12} and the negative magnetoresistance^{12,14}. However, a direct observation of overlapping polarons in EuB_6 has so far been elusive.

In this paper we present the results of μSR experiments on EuB_6 which not only provide further evidence for the two distinct magnetic transitions but are also able

to resolve two components arising from muons stopping in two different types of environment below T_m . The first component is an oscillating signal and can be associated with muons that stop in a locally ferromagnetic environment. The second component is a Gaussian signal and arises from the muons that come to rest in a paramagnetic environment. This provides clear evidence for magnetic phase separation below T_m .

Our μSR experiments were carried out using the DOLLY instrument at the Paul Scherrer Institute (PSI) in Switzerland and the DEVA beamline at the ISIS pulsed muon facility in the UK. In our μSR experiments, spin polarised positive muons (μ^+ , mean lifetime $2.2 \mu\text{s}$, momentum $28 \text{ MeV}/c$) were implanted into polycrystalline EuB_6 . The muons stop quickly (in $< 10^{-9}$ s), without significant loss of spin-polarisation. The time evolution of the muon spin polarisation can be detected by counting emitted decay positrons forward (f) and backward (b) of the initial muon spin direction due to the asymmetric nature of the muon decay¹⁵. In our experiments, positrons are detected using scintillation counters placed in front of and behind the sample. We record the number of positrons detected by forward (N_f) and backward (N_b) counters as a function of time and calculate the asymmetry function, $G_z(t)$, using

$$G_z(t) = \frac{N_f(t) - \alpha_{\text{exp}} N_b(t)}{N_f(t) + \alpha_{\text{exp}} N_b(t)}, \quad (1)$$

where α_{exp} is an experimental calibration constant and differs from unity due to non-uniform detector efficiency. The quantity $G_z(t)$ is then proportional to the average spin polarisation, $P_z(t)$, of muons stopping within the sample. The muon spin precesses around a local magnetic field, B (with a frequency $\nu = (\gamma_\mu/2\pi)|B|$, where $\gamma_\mu/2\pi = 135.5 \text{ MHz T}^{-1}$).

Examples of asymmetry spectra measured at PSI are shown in Fig. 1. There are three distinct temperature regions. In the lowest temperature data ($T \lesssim 10$ K), there are clear oscillations in the measured asymmetry, demonstrating that the sample does indeed make a transition

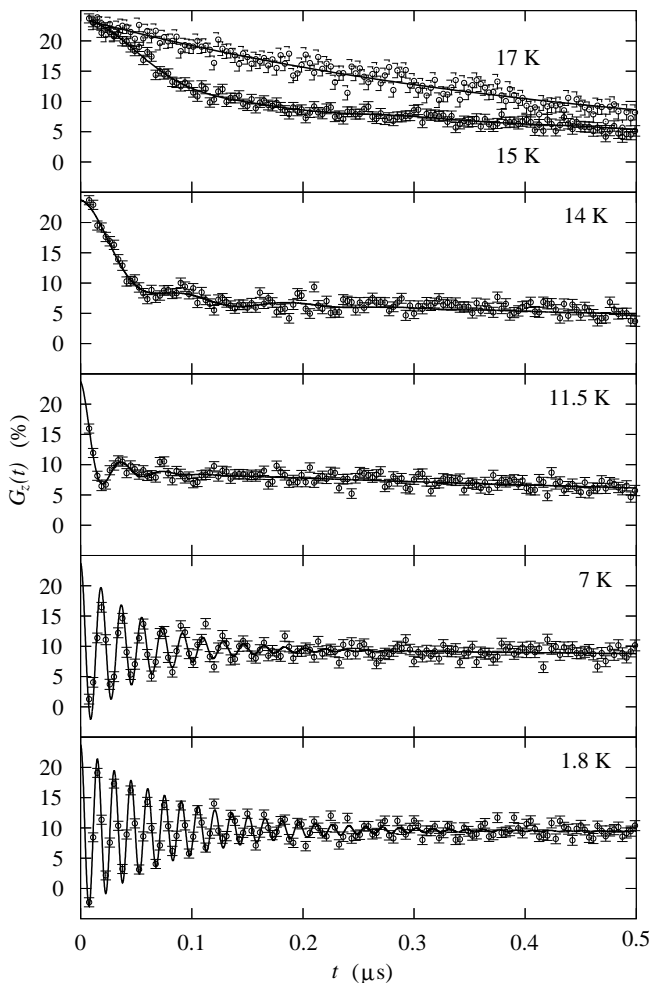


FIG. 1: Muon decay asymmetry plots for EuB_6 at different temperatures. The solid lines are fits of the data to Eq. 2. The data for $T = 11.5, 14$ and 15 K are fitted with a non-zero Gaussian amplitude, whilst the others are not. The data were taken at PSI.

to a locally magnetically ordered state. This oscillating signal is superposed on a slow exponential relaxation unobservable in Fig. 1, but visible at longer times. In the second region ($10 \text{ K} \lesssim T < T_m$), the amplitude of the oscillatory component decreases and a Gaussian component appears, with a decay rate that decreases as the temperature is increased. In the third region ($T > T_m$), the amplitude associated with the Gaussian component decreases until, when above 16 K , only the slow exponential relaxation remains. The need for the fast relaxing Gaussian term in the fits is clearly motivated by the topmost panel of Fig. 1, where the purely exponential relaxation seen at 17 K is compared with the results for a temperature of 15 K , which is just inside the intermediate region.

In order to best follow these changes, the data over the whole studied temperature range were fitted to the

function

$$G_z(t) = A_{\text{exp}} \exp\left(-\frac{t}{T_1}\right) + A_{\text{osc}} \exp\left(-\frac{t}{T_2}\right) \cos(2\pi\nu t) + A_{\text{gauss}} \exp(-\sigma^2 t^2) + A_{\text{bg}}, \quad (2)$$

where A_{bg} represents a time-independent background due to muons stopping in the silver that surrounds the sample, T_1 and T_2 are the longitudinal and transverse relaxation times, and A_{exp} , A_{osc} and A_{gauss} are the amplitudes of the exponential, oscillating and Gaussian terms respectively. Plots of the fitted parameters against temperature are shown in Fig. 2. Vertical lines drawn at T_m and T_c approximately divide the plots into the three temperature regions discussed above. In Fig. 2(e) the asymmetry amplitudes of the three different terms are shown, which provide the main motivation for this division. The exponentially relaxing fraction is seen to drop sharply from the maximum value at T_m ; this is expected in a polycrystalline sample when a transition into an ordered state occurs. In the lowest temperature region the remaining amplitude is accounted for by the oscillating fraction, so that here the sample is uniformly magnetically ordered, but at intermediate temperatures there is also a contribution from the fast relaxing Gaussian fraction.

The fact that the asymmetry amplitude is shared between the two fast signals in the intermediate region is evidence that the muons are stopping in two different kinds of environment, that is, magnetic phase separation is occurring^{16,17}. The amplitudes of the two signals are expected to be proportional to the volume fraction of each phase. Phase separation is important between T_m and T_c , but we find it disappears below T_c , in contrast to the predictions of Ref. 17.

A Gaussian relaxation can result from a field at the muon site which is static but randomly distributed in magnitude. The parameter σ is related to the width of the field distribution as $\sigma^2 = \gamma_\mu^2 \langle B^2 \rangle / 2$. Fig. 2(d) shows that σ increases as the temperature is lowered in the second region, indicating that the field distribution at the muon sites is becoming wider as the sample becomes more ordered at lower temperatures.

Fig. 2(a) shows that the oscillations develop below T_m , and their frequency ν increases fairly smoothly as the sample is cooled through T_c rising to a maximum of $\sim 67 \text{ MHz}$ at low temperature (corresponding to a field at the muon site of $\sim 0.5 \text{ T}$). The frequency ν is proportional to the magnetization and the data in Fig. 2(a) match well with the temperature dependence of the Eu magnetic moment measured with neutron scattering³. Only one muon precession frequency is observed, strongly suggesting that there is a single set of equivalent muon sites in the structure. There are two candidate sites. The first is at the centre of a B_6^{2-} octahedron, and the second is at the face-centres of the unit cell (in the centre of the shortest B-B bond which is between atoms in adjacent unit cells). Using the Eu moment measured previously³ and assuming a low temperature magnetic

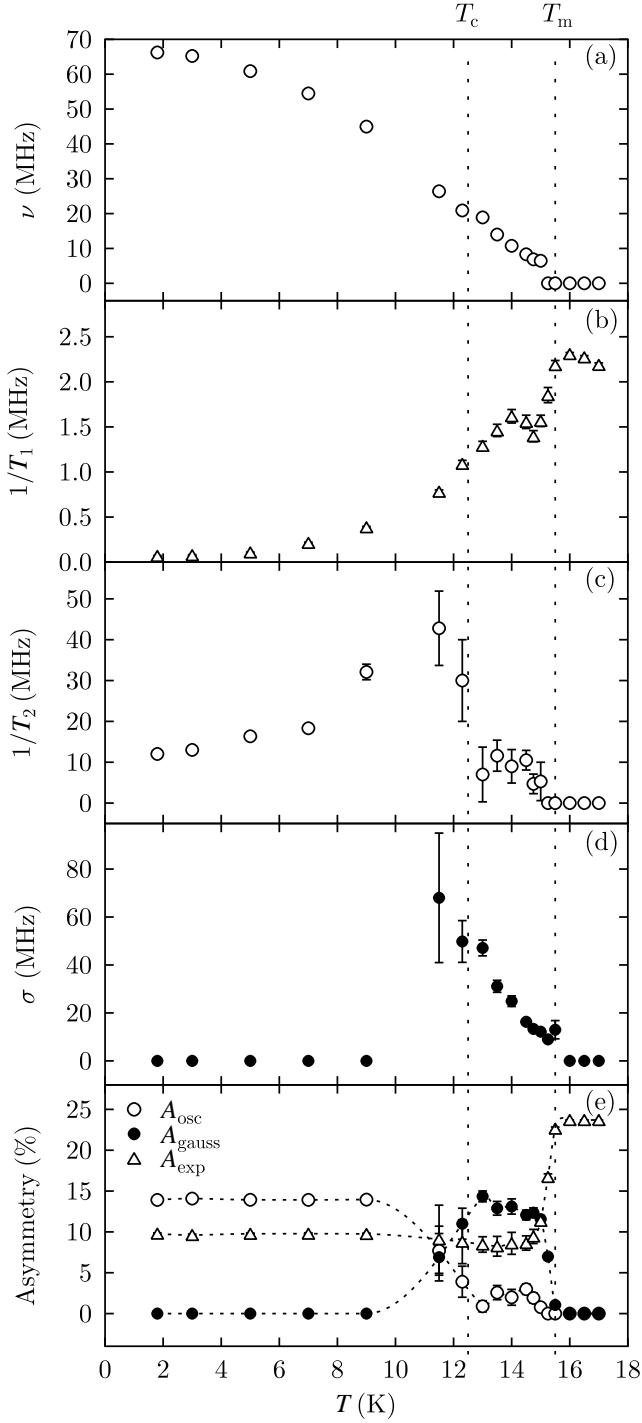


FIG. 2: Temperature dependence of the parameters determined from fits of Eq. 2 to EuB_6 asymmetry spectra. The panels correspond to (a) the oscillation frequency, ν , (b) and (c) the relaxation rates $1/T_1$ and $1/T_2$, (d) the Gaussian fraction width parameter, σ , and (e) the amplitudes for each of the three components used in the fits. The dashed lines in (e) are guides for the eye. The vertical dashed lines indicate the positions of T_c and T_m .

structure with the moments pointing along the [111] direction, the dipole field (\mathbf{B}_{dip}) can be calculated at both these possible sites. At the centre of a boron octahedron, the dipole field cancels by symmetry. The face-centre positions are all magnetically equivalent and yield $\gamma_\mu |\mathbf{B}_{\text{dip}}|/2\pi = 144 \text{ MHz}$. Additional contributions to the field at the muon site arise from the Lorentz field ($\mu_0 M_{\text{sat}}/3 = 0.42 \text{ T}$, corresponding to 57 MHz), the demagnetization field and the hyperfine contact field, and preclude a definitive assignment of the site.

The longitudinal relaxation rate, $1/T_1$, reflects the dynamics of the fields being probed. For rapid fluctuations, $1/T_1 \propto \gamma_\mu^2 \sum_q |\delta B(q)|^2 \tau(q)$, where $|\delta B(q)|$ is the amplitude of the fluctuating local field and $\tau(q)$ is the Eu-ion correlation time at wavevector q . In the paramagnetic phase the spin fluctuations are so rapid that the measured relaxation rate is small. As the sample is cooled and the critical region is approached, the correlation time becomes longer and the relaxation rate rises and peaks close to T_m (Fig. 2(b)). In contrast, $1/T_2$ (which is proportional to the width of the ordered field distribution corresponding to the oscillating fraction) rises dramatically on cooling through T_c and subsequently falls on further cooling (Fig. 2(c)). This emphasises that the ordered and fluctuating fractions in the sample are distinct and follow different temperature dependences.

These observations fit in well with the polaron percolation picture for the intermediate temperature range; muons stopping in ferromagnetic regions of overlapping polarons give rise to the oscillating signal, while most muons stop in the intervening paramagnetic regions. In these paramagnetic regions the Eu-ion correlation time is short, so the muons are not depolarized by the local fluctuating Eu moments, but by the distribution of fields that result from the nearby ferromagnetic regions. As the sample becomes more ordered the paramagnetic regions shrink, with a corresponding effect on the field distribution.

In order to study the slower relaxation in the high temperature region in more detail, data were collected at the ISIS facility. An example is shown in Fig. 3(a) and clearly shows the presence of both a slow and a fast relaxation rate. Therefore the data were fitted to the function¹⁸

$$G_z(t) = A_f \exp(-\lambda_f t) + A_s \exp(-\lambda_s t) + A_{\text{bg}}, \quad (3)$$

where $A_{f,s}$ and $\lambda_{f,s}$ are the amplitudes and relaxation rates of the fast and slow exponential components (note that λ_f represents relaxation due to *fast* dynamics and hence *slow* spin relaxation). The non-relaxing background fraction A_{bg} was held fixed. A_f and A_s were found to be approximately constant with temperature, with A_f about half the value of A_s , and were fixed in the fits. The relaxation rates themselves appear temperature independent above the transition, and it was possible to keep λ_f fixed at 0.08 MHz (see Fig. 3). On cooling towards T_c , λ_s begins to decrease, until only one relaxation rate can be resolved below 9 K . This is possibly because the two rates become very similar in magnitude, and the

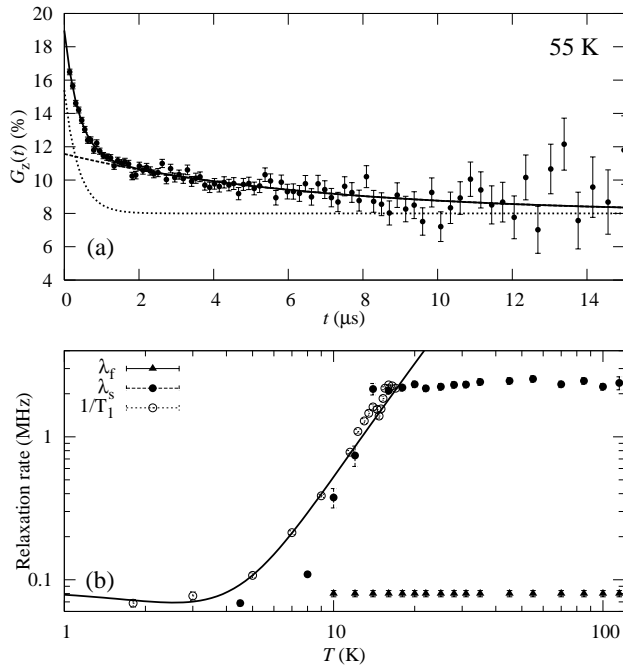


FIG. 3: Panel (a) shows a typical asymmetry spectrum measured at ISIS. The solid line is a fit to Eq. 3, and the dotted lines show the form of the two exponential terms used. Panel (b) shows the two relaxation rates measured at ISIS, $\lambda_{f,s}$ (filled symbols), and the longitudinal relaxation rate measured at PSI, $1/T_1$ (open symbols). The solid line is a fit of a $T^2 \ln(T/\Delta)$ function to the PSI rate for temperatures below 14 K.

presence of λ_f may mask any further drop of λ_s .

The relaxation rate λ_s matches well with the temperature dependence of $1/T_1$, as shown in Fig. 3(b), and the two can be identified with each other. At low

temperatures, a contribution to $1/T_1$ can be fitted by $1/T_1 \propto T^2 \ln(T/\Delta)$ (see Fig. 3(b)), appropriate for scattering by two-magnon processes in ferromagnets¹⁹. However, the component due to fast fluctuations produces too slow a relaxation to be convincingly included in the fits to the PSI data. Nevertheless, the observation of two relaxation rates above T_m allows us to infer the presence of spatial inhomogeneity (a very similar effect has been found in $\text{La}_{0.67}\text{Ca}_{0.33}\text{MnO}_3$ with μSR ¹⁸), which persists even at 115 K. Above T_m , the temperature dependence of λ_f and λ_s is weak and featureless. Any polaron dynamics are presumably too fast to be followed by the muon. The dramatic changes observed below T_m can therefore be attributed to a large change in the time-scale of polaron dynamics, such as might be expected when polarons overlap. Although the polaron volume fraction changes little at a percolation transition, their arrangement could be changed so that the average size of a single polaron is larger and its dynamics are much slower.

In conclusion, μSR measurements have allowed us to follow the very unusual development of ferromagnetism in EuB_6 through the transitions at T_m and T_c from a local viewpoint. These results reveal two distinct and spatially separate regions of the material associated with different magnetic behaviour. Such magnetic phase separation is qualitatively consistent with a picture based on coalescing polarons.

Part of this work was performed at the Swiss Muon Source, Paul Scherrer Institute, Villigen, Switzerland and the ISIS pulsed muon source, RAL, UK. We are grateful to Robert Scheuermann and Steve Cottrell for experimental assistance and Maria Calderón and Amalia Coldea for useful discussions. This work was funded by the EPSRC (UK) and the NSF under grant DMR-0203214

- ¹ Z. Fisk, D. C. Johnston, B. Cornut, S. von Molnar, S. Oseroff, and R. Calvo, J. Appl. Phys. **50**, 1911 (1979).
- ² S. Süllow, I. Prasad, M. C. Aronson, S. Bogdanovich, J. L. Sarrao, and Z. Fisk, Phys. Rev. B **62**, 11626 (2000).
- ³ S. Süllow, I. Prasad, M. C. Aronson, J. L. Sarrao, Z. Fisk, D. Hristova, A. H. Lacerda, M. F. Hundley, A. Vigliante, and D. Gibbs, Phys. Rev. B **57**, 5860 (1998).
- ⁴ W. Henggeler, H.-R. Ott, D. P. Young, and Z. Fisk, Solid State Commun. **108**, 929 (1998).
- ⁵ C. N. Guy, S. v. Molnar, J. Etourneau, and Z. Fisk, Solid State Commun. **33**, 1055 (1980).
- ⁶ S. Massidda, A. Continenza, T. M. de Pascale, and R. Monnier, Z. Phys. B: Condensed Matter **102**, 83 (1996).
- ⁷ M. C. Aronson, J. L. Sarrao, Z. Fisk, M. Whitton, and B. L. Brandt, Phys. Rev. B **59**, 4720 (1999).
- ⁸ R. G. Goodrich, N. Harrison, J. J. Vuillemin, A. Teklu, D. W. Hall, Z. Fisk, D. Young, and J. Sarrao, Phys. Rev. B **58**, 14896 (1998).
- ⁹ J. Kuně and W. E. Pickett, Phys. Rev. B **69**, 165111 (2004).

- ¹⁰ G. A. Wigger, R. Monnier, H. R. Ott, D. P. Young, and Z. Fisk, Phys. Rev. B **69**, 125118 (2004).
- ¹¹ M. Imada, A. Fujimori, and Y. Tokura, Rev. Mod. Phys. **70**, 1039 (1998).
- ¹² M. J. Calderón, L. G. L. Wegener, and P. B. Littlewood, cond-mat/0312437 (2003).
- ¹³ P. Nyhus, S. Yoon, M. Kauffman, S. L. Cooper, Z. Fisk, and J. Sarrao, Phys. Rev. B **56**, 2717 (1997).
- ¹⁴ J. Chatterjee, U. Yu, and B. I. Min, Phys. Rev. B **69**, 134423 (2004).
- ¹⁵ S. J. Blundell, Comtemp. Phys. **40**, 175 (1999).
- ¹⁶ K. H. Kim, M. Uehara, V. Kiryukhin, and S.-W. Cheong, cond-mat/0212113 (2002).
- ¹⁷ I. Y. Korenblit, Phys. Rev. B **64**, 100405 (2001).
- ¹⁸ R. H. Heffner, J. E. Sonier, D. E. MacLaughlin, G. J. Nieuwenhuys, G. Ehlers, F. Mezei, S.-W. Cheong, J. S. Gardner, and H. Röder, Phys. Rev. Lett. **85**, 3285 (2000).
- ¹⁹ A. Yaouanc and P. D. de Réotier, J. Phys.: Condens. Matter **3**, 6195 (1991).